UDC 621.314 https://doi.org/10.20998/2074-272X.2024.2.06

H.K.E. Zine, K. Abed

Smart current control of the wind energy conversion system based permanent magnet synchronous generator using predictive and hysteresis model

Introduction. *Given the increasing demand for performance and efficiency of converters and power drives, the development of new control systems must take into account the real nature of these types of systems. Converters and dimmers power are nonlinear systems of a hybrid nature, including elements linear and nonlinear and a finite number of switching devices. Signals input for power converters are discrete signals that control the 'opening and closing' transitions of each component.* ***Problem.*** *In the multilevel inverters connected to grid, the switching frequency is the principal cause of harmonics and switching losses, which by nature, reduces the inverter's efficiency.* ***Purpose.*** *For guarantee the satisfying quality of power transmitted to the electrical grid, while ensuring reduction of current ripples and output voltage harmonics.* ***Novelty.*** *This work proposes a new smart control, based on a predictive current control of the three level neutral point clamped inverter, used in Wind Energy Conversion System (WECS) connected to grid, based permanent magnet synchronous generator, powered by a hysteresis current control for the rectifier. This new formula guarantees handling with the influence of harmonics disturbances (similar current total harmonic distortion), voltage stress, switching losses, rise time, over or undershoot and settling time in WECS.* ***Methods.*** *The basic idea of this control is to choose the best switching state, of the power switches, which ameliorates the quality function, selected from order predictive current control of WECS.* ***Results. Practical value.*** *Several advantages in this intelligent method, such as the fast dynamic answer, the easy implementation of nonlinearities and it requires fewer calculations to choose the best switching state. In addition, an innovative algorithm is proposed to adjust the current ripples and output voltage harmonics of the WECS. The performances of the system were analyzed by simulation using MATLAB/Simulink.* References 33, table 3, figures 11.

Key words: **hysteresis current control, permanent magnet synchronous generator, predictive current control, wind energy conversion system, three level neutral point clamped inverter.**

Вступ. *Зважаючи на зростаючі вимоги до продуктивності та ефективності перетворювачів та силових приводів, при розробці нових систем керування необхідно враховувати реальну природу систем такого типу. Перетворювачі та регулятори потужності являють собою нелінійні системи гібридної природи, що включають лінійні та нелінійні елементи та кінцеве число комутаційних пристроїв. Вхідні сигнали для силових перетворювачів є дискретними сигналами, які керують переходами «відкриття та закриття» кожного компонента.* ***Проблема***. *У багаторівневих інверторах, підключених до мережі, частота перемикання є основною причиною гармонік та втрат перемикання, що за своєю природою знижує ефективність інвертора.* ***Мета***. *Гарантувати задовільну якість електроенергії, що передається в електричну мережу, при одночасному зниженні пульсацій струму та гармонік вихідної напруги.* ***Новизна***. *У цій роботі пропонується новий інтелектуальний контроль, заснований на прогнозуючому керуванні струмом трирівневого інвертора з фіксованою нейтральною точкою, що використовується в системі перетворення енергії вітру (WECS), підключеної до мережі, на основі синхронного генератора з постійними магнітами, що живиться від керування струмом . Ця нова формула гарантує обробку з урахуванням впливу гармонічних перешкод (аналогічні загальні гармонічні спотворення струму), перенапруги, втрат перемикання, часу наростання, пере- чи недорегулювання, а також часу стабілізації WECS.* ***Методи***. *Основна ідея цього управління полягає у виборі найкращого стану перемикання силових перемикачів, що покращує функцію якості, обрану з порядку прогнозуючого керування струмом WECS.* ***Результати***. ***Практична цінність***. *Цей інтелектуальний метод має кілька переваг, таких як швидка динамічна відповідь, простота реалізації нелінійностей і необхідність меншої кількості обчислень для вибору найкращого стану перемикання. Крім того, запропоновано інноваційний алгоритм регулювання пульсацій струму та гармонік вихідної напруги WECS. Характеристики системи проаналізовано шляхом моделювання з використанням MATLAB/Simulink.* Бібл. 33, табл. 3, рис. 11.

Ключові слова: **управління струмом з гістерезисом, синхронний генератор з постійними магнітами, прогностичне управління струмом, система перетворення енергії вітру, інвертор з трирівневим фіксуванням нейтральної точки.**

Introduction. The increasing use in the industrial sector of powered systems electronically and controllable, motivated by the improvement of their performance, has led to a proliferation of static converters. Among these most common structures and the most attractive are the Pulse Width Modulation (PWM) voltage rectifier [1].

Participation in system services must be on an alternative grid three-phase. It is then necessary to use an electronic converter for the DC-AC and/or AC-DC conversion in the conversion chain wind energy [1, 2].

The advent of power electronics has a major impact on the world of industry in recent decades. This advent occurred through the arrival on the market for power electronic components such as thyristors, triacs, GTO, IGBT or high-power transistors.

The constant growth of energy consumption in all its forms and the associated polluting effects, mainly caused by the combustion of fossil fuels, are at the heart of the issue of sustainable development and care of the environment in a discussion for the future of the planet.

Wind energy is clean and renewable energy, unlike conventional energy which presents the constraints of distance from the electricity network and the constraints of fuel transport, as well as the periodic maintenance of the installations [3].

In recent literatures, authors have investigated the potential technical impacts in voltage regulation, active and reactive power variations, transformers loading, current and voltage harmonics causes with renewable energy integration [4-6].

In the resolution of harmonics disturbances problems, many researchers used the sinusoidal PWM approach and implement it in Wind Energy Conversion System (WECS) to ameliorate the harmonic content on the output voltage waveform [7]. Space vector modulation technique possesses remarkable performance in 3-level PWM topologies [8]. Other techniques involving modulation methods at a low switching frequency that have attained more demand in a broader field of function are staircase modulation, space vector control [9, 10], selective harmonic elimination [10, 11] and sliding mode control for Permanent Magnet Synchronous Generator (PMSG) [12].

System for application generator. In the studied system, we are interested in the wound rotor PMSG and its use for the production of electrical energy from wind power. The variable speed configuration is represented in Fig. 1.

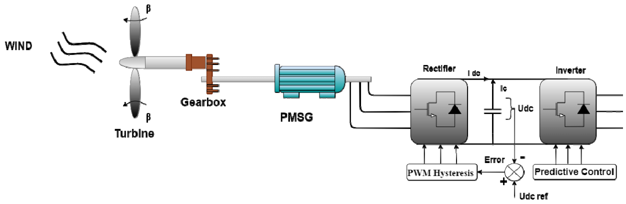

Fig. 1. PMSG-based WECS

The rotor is connected to a rectifier (rotor side converter). A predictive control applied to Three Level Neutral Point Clamped (3L-NPC) inverter (grid side converter), which is placed in the output of the rectifier controlled by PWM hysteresis.

1. The modeling of the turbine. The turbine rotate speed is depending on wind speed; this makes it possible to know the wind torque applied to the wind turbine. This modeling is based on bibliographic cross-checking or additional information from brochures from different manufacturers [13]:

$$P_{aer} = \frac{1}{2} c_p(\lambda,\beta)\rho S V_v^3 = \frac{1}{2}\rho\pi R_t^2 V_v^3, \qquad (1)$$

where

$$\lambda = \frac{\Omega_t R_t}{V_v}, \qquad (2)$$

where P_{aer} is the aerodynamic power; c_p indicates the performance coefficient of the wind generator; λ is the speed ratio (rad); β is the inclination angle of the blade, which depicts the orientation angle of the blades; Ω_t is the turbine rotation speed; R_t is the blade radius; V_v is the wind speed; ρ is the air density (1.22 kg/m^3 at atmospheric pressure at 15 °C); the Betz limit is that the coefficient $c_p(\lambda, \beta)$ does not exceed the value 16/17=0.59 [13, 14].

2. Modeling of the multiplier. The multiplier adapts the turbine rotation speed to the PMSG rotation speed. For this we grant a multiplier between the turbine and the PMSG, the latter is mathematically modelled by the following equations:

$$C_g = C_t / G \quad (3) \qquad \text{and} \qquad \Omega_t = \Omega_{mech} / G. \quad (4)$$

The mechanical equations:

$$\frac{C_t}{G} - C_g = \left(\frac{J_t}{G^2} + J_g\right)\frac{\mathrm{d}\Omega_{mech}}{\mathrm{d}t} + \left(\frac{f_t}{G^2} + f_g\right)\Omega_{mech}; \quad (5)$$

$$\frac{J_t}{G^2} + J_g = J \quad (6) \qquad \text{and} \qquad \frac{f_t}{G^2} + f_g = f. \quad (7)$$

So, the mechanical equations are:

$$C_{mech} = J\frac{\mathrm{d}\Omega_{mech}}{\mathrm{d}t}; \qquad (8)$$

$$C_{mech} = C_g - C_{em} - C_{vis}; \qquad (9)$$

$$C_{vis} = f\Omega_{mech}, \qquad (10)$$

where C_{mech}, C_t, C_g, C_{vis} are the mechanical, wind, electromagnetic and viscous torques, respectively; J, J_t, J_g are the total, turbine and generator inertias; f, f_t, f_g are the coefficient of total friction, viscous friction of the turbine and of the generator; G is the ratio of the speed multiplier; Ω_{mech} is the generator rotation speed (fast axis).

3. PMSG modeling. By choosing a *d-q* reference frame synchronized with the stator flux [3, 14, 15] are next.

The equations of tensions:

$$\begin{cases} V_{sd} = R_s I_{sd} + \dfrac{\mathrm{d}\varphi_{sd}}{\mathrm{d}t} - \omega_s\varphi_{sq}; \\ V_{sq} = R_s I_{sq} + \dfrac{\mathrm{d}\varphi_{sq}}{\mathrm{d}t} - \omega_s\varphi_{sd}; \\ V_{rd} = R_r I_{rd} + \dfrac{\mathrm{d}\varphi_{rd}}{\mathrm{d}t} - (\omega_s - \omega)\varphi_{rq}; \\ V_{rq} = R_r I_{rq} + \dfrac{\mathrm{d}\varphi_{rq}}{\mathrm{d}t} - (\omega_s - \omega)\varphi_{rd}; \\ J\dfrac{\mathrm{d}\Omega_t}{\mathrm{d}t} = C_{em} - C_r - f_r\Omega_r, \end{cases} \qquad (11)$$

The equations of the flux:

$$\begin{cases} \varphi_{sd} = L_s I_{sd} + M I_{rd}; \\ \varphi_{sq} = L_s I_{sq} + M I_{rq}; \\ \varphi_{rd} = L_r I_{rd} + M I_{sd}; \\ \varphi_{rq} = L_r I_{rq} + M I_{sq}, \end{cases} \qquad (12)$$

$$C_{em} = \frac{M}{L_r} p\left(\varphi_{dr} I_{qs} - \varphi_{qr} I_{ds}\right). \qquad (13)$$

The electromagnetic torque becomes:

$$C_{em} = \frac{3}{2}\frac{M}{L_s} p\left(\varphi_{qs} I_{dr} - \varphi_{ds} I_{qr}\right). \qquad (14)$$

The stator and rotor active and reactive powers are expressed by:

$$\begin{cases} P_s = \dfrac{3}{2}\left(V_{sd} I_{sd} + V_{sq} I_{sq}\right); \\ Q_s = \dfrac{3}{2}\left(V_{sq} I_{sd} + V_{sd} I_{sq}\right); \\ P_r = \dfrac{3}{2}\left(V_{rd} I_{rd} + V_{rq} I_{rq}\right); \\ Q_r = \dfrac{3}{2}\left(V_{rq} I_{rd} + V_{rd} I_{rq}\right), \end{cases} \qquad (15)$$

where R_s, R_r are the stator and rotor resistances; L_s, L_r, M are the stator, rotor, mutual inductances, respectively; I_{sd}, I_{sq}, I_{rd}, I_{rq} are the stator and rotor currents in the *d-q* frame; φ_{sd}, φ_{sq}, φ_{rd}, φ_{rq} are the stator and rotor flux in the *d-q* frame; p is the number of pairs of poles; P_s, Q_s, P_r, Q_r are the stator and rotor active and reactive powers; V_{sd}, V_{sq}, V_{rd}, V_{rq} are the stator and rotor voltage components in the *d-q* frame; ω_s is the speed of stator magnetic field; $\omega_r = \omega_s - \omega$ is the angular speed of rotor; ω is the mechanical angular speed.

PMSG and turbine parameters are shown in Table 1.

Table 1

PMSG and turbine parameters

PMSG parameters		Turbine parameters
P_n = 1680 W	L_1 = 0.6 mH	R = 1.8 m
V_s = 110 V	L_s = 5.25 mH	J = 0.07 kg·m^2
f = 50 Hz	ω_r = 0.1827 rad/s	G = 1
R_s = 0.9585 Ω	C = 8 N·m	ρ = 1.25 kg/m^3
R_1 = 0.5 Ω	p = 4	

Hysteresis current control.

1. Modeling of the rectifier. The rectifier bridge consists of three arms with six bipolar transistors antiparallel with diodes. These switches are controlled by closing and opening (pulse time closing «0» and opening «1»). And in the same arm the switches operate in a complementary way ($K_a = \overline{K'_a}$) to avoid the short circuit [16]. The model of bridge rectifier is depicted in Fig. 2.

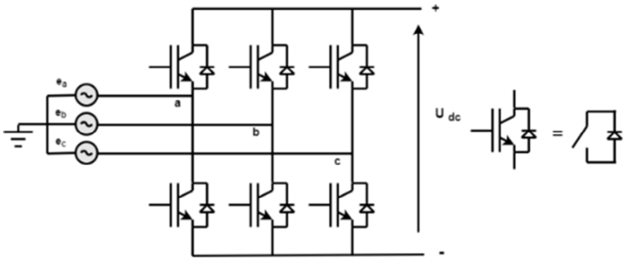

Fig. 2. Bridge rectifier

The different switching and combination states of the PWM rectifier switches are shown in Table 2.

Table 2

8 possible states of the switches

K	S_a	S_b	S_c	V_{ab}	V_{bc}	V_{ac}
0	1	0	0	U_{dc}	0	$-U_{dc}$
1	1	1	0	0	U_{dc}	$-U_{dc}$
2	0	1	1	$-U_{dc}$	U_{dc}	0
3	0	1	0	$-U_{dc}$	0	U_{dc}
4	0	0	1	0	$-U_{dc}$	U_{dc}
5	1	0	1	U_{dc}	$-U_{dc}$	0
6	0	0	0	0	0	0
7	1	1	1	0	0	0

From Table 1 we can represent the rectifier input voltages in general as follows [17-19]:

$$V_{ab} = (S_a - S_b)U_{dc}; \quad (16)$$

$$V_{bc} = (S_b - S_c)U_{dc}; \quad (17)$$

$$V_{ca} = (S_c - S_a)U_{dc}. \quad (18)$$

So we can deduce the phase-to-neutral voltages:

$$V_b = f_b U_{dc}; \quad (19)$$

$$V_c = f_c U_{dc}, \quad (20)$$

where:

$$f_a = \frac{2S_a - (S_b + S_c)}{3}; \quad (21)$$

$$f_b = \frac{2S_b - (S_a + S_c)}{3}; \quad (22)$$

$$f_c = \frac{2S_c - (S_a + S_b)}{3}. \quad (23)$$

8 possible states of the input voltage V in a complex plane α-β [20]:

$$V_{k+1} = \begin{cases} \frac{2}{3} U_{dc} e^{\frac{jk\pi}{3}} & \text{for } k = 0 \ldots 5; \\ V_7 = V_0 = 0. \end{cases} \quad (24)$$

8 voltage vectors noted as $V_0(0\ 0\ 0) - V_7(1\ 1\ 1)$ are presented in Fig. 3, where V_{ab}, V_{bc}, V_{ca} are the complex voltages; f_a, f_b, f_c are the rectifier switching function; U_{dc} is the rectified voltage; S_a, S_b, S_c are the switching states of the rectifier; V_a, V_b, V_c are the simple voltages.

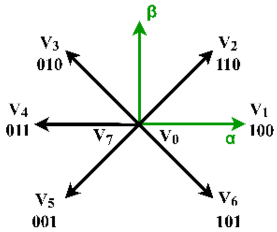

Fig. 3. Presentation of voltage vector V_k

2. Functional representation of the PWM rectifier in the three-phase reference. The voltage equations for the balanced three-phase system without neutral can be written as (Fig. 3):

$$\bar{e} = \overline{V_1} + \overline{V}; \quad (25)$$

$$\bar{e} = R\bar{i} + L\frac{\mathrm{d}\bar{i}}{\mathrm{d}t} + \overline{V}; \quad (26)$$

$$\begin{bmatrix} e_a \\ e_b \\ e_c \end{bmatrix} = R\begin{bmatrix} i_a \\ i_b \\ i_c \end{bmatrix} + L\frac{\mathrm{d}}{\mathrm{d}t}\begin{bmatrix} i_a \\ i_b \\ i_c \end{bmatrix} + \begin{bmatrix} V_a \\ V_b \\ V_c \end{bmatrix}; \quad (27)$$

The rectifier input voltage can be written as:

$$V_n = U_{dc}\left(S_n \cdot \frac{1}{3} \cdot \sum_{n=a}^{c} S_n\right), \quad (28)$$

where S_n = 0 or 1 are the state of the switches, where ($n = a, b, c$). In addition, we can write the DC bus current as:

$$C\frac{\mathrm{d}U_{dc}}{\mathrm{d}t} = i_c. \quad (29)$$

The current in the capacitor can also write:

$$i_c = i_{dc} - i_{ch}; \quad (30)$$

$$C\frac{\mathrm{d}U_{dc}}{\mathrm{d}t} = S_a i_a + S_b i_b + S_c i_c - i_{dc}. \quad (31)$$

Also, the current i_c is the sum of the currents of each phase by the state of its switch [16]:

$$C\frac{\mathrm{d}U_{dc}}{\mathrm{d}t} = S_a i_a + S_b i_b + S_c i_c - i_{ch}. \quad (32)$$

So, the AC side of the rectifier:

$$L\frac{\mathrm{d}i_a}{\mathrm{d}t} + Ri_a = e_a - U_{dc}\left(S_a - \frac{1}{3}\cdot\sum_{n=a}^{c} S_n\right) = e_a - U_{dc}\left(S_a - \frac{1}{3}(S_a + S_b + S_c)\right); \quad (33)$$

$$L\frac{\mathrm{d}i_b}{\mathrm{d}t} + Ri_b = e_b - U_{dc}\left(S_b - \frac{1}{3}\cdot\sum_{n=a}^{c} S_n\right) = e_b - U_{dc}\left(S_b - \frac{1}{3}(S_a + S_b + S_c)\right); \quad (34)$$

$$L\frac{\mathrm{d}i_c}{\mathrm{d}t} + Ri_c = e_c - U_{dc}\left(S_c - \frac{1}{3}\cdot\sum_{n=a}^{c} S_n\right) = e_c - U_{dc}\left(S_c - \frac{1}{3}(S_a + S_b + S_c)\right), \quad (35)$$

where the network voltages are expressed by:

$$e_a = E_m \sin(\omega t); \quad (36)$$

$$e_b = E_m \sin(\omega t - 2\pi/3); \quad (37)$$

$$e_c = E_m \sin(\omega t + 2\pi/3). \quad (38)$$

The above equation can be summarized as:

$$L\frac{\mathrm{d}i_n}{\mathrm{d}t}+Ri_n=e_n-U_{dc}\left(S_n-\frac{1}{3}\cdot\sum_{n=a}^{c}S_n\right); \qquad (39)$$

$$C\frac{\mathrm{d}U_{dc}}{\mathrm{d}t}=\sum_{n=a}^{c}i_nS_n-i_{ch}, \qquad (40)$$

where e_a, e_b, e_c are the network voltages; V_n are the instantaneous phase voltages; S_n are the switching states; i_c is the capacitor current; i_{dc} is the rectifier output current; i_{ch} is the load current; E_m is the maximum phase voltage.

3. PWM to hysteresis band. The purpose of hysteresis controller is to force the actual current to follow the predefined reference current. In conventional hysteresis controller, the comparators switch between the fixed bandwidths, this technique only requires a hysteresis comparator per phase [21, 22].

The principle of hysteresis used in this system is expressed in Fig. 4. The switch opens if the error becomes less than *–H*/2, it closes if the latter is greater than *+H*/2, where *H* is the range (or width) of hysteresis. If the error is now between *–H*/2, and *+H*/2, (it varies within the hysteresis range), the switch does not switch [21, 23].

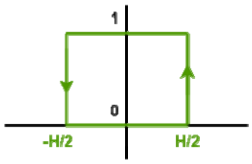

Fig. 4. Diagram of proposed hysteresis controller

The topology of hysteresis current control PWM technique using in this configuration is shown in Fig. 5.

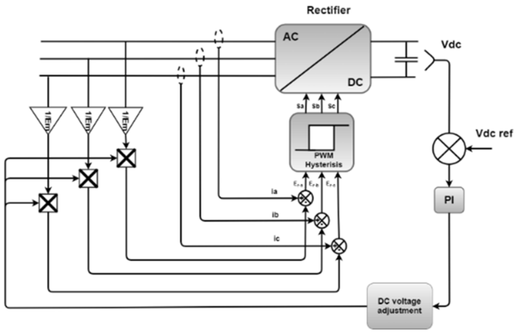

Fig. 5. Control diagram of the hysteresis current control rectifier connected to the inverter

Implementation predictive current control 3L-NPC inverter.

1. Modeling inverter 3L-NPC. The power and control circuit of a 3L-NPC inverter connected to grid is shown in Fig. 6, each phase of three-phase 3L-NPC inverter consists of 3 arms constituted of 4 switches (S1, S2, S3, S4) connected in series and 2 median diodes (D1 and D2). The midpoints of switches (S2 and S3) of each phase are connected to the load and the midpoints of diodes (D1 and D2) are connected to the neutral point [24, 25].

In the same arm the switches operate in a complementary way connection functions of the arm switches *k* (a complementary way) will be given by:

$$\overbrace{\begin{cases}S_{a1}=\overline{S_{a2}}\\ S_{a3}=\overline{S_{a4}}\end{cases}\quad\begin{cases}S_{a1}=\overline{S_{a3}}\\ S_{a2}=\overline{S_{a4}}\end{cases}\quad\begin{cases}S_{a1}=\overline{S_{a4}}\\ S_{a2}=\overline{S_{a3}}\end{cases}}. \qquad (41)$$

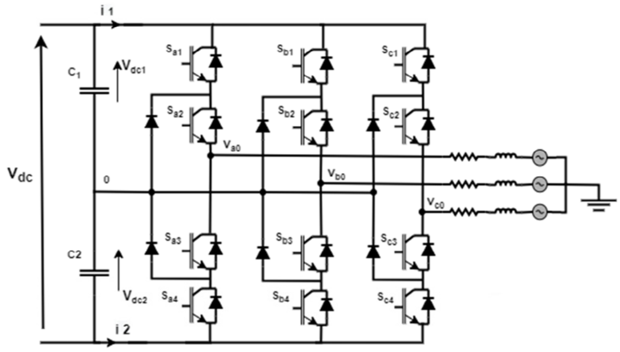

Fig. 6. The power circuit model of a 3L-NPC inverter connected to the grid

The switching function on *A*, *B*, and *C* phase can be defined as follows:

$$\overbrace{\begin{cases}S_{k1}=\overline{S_{k3}}\\ S_{k2}=\overline{S_{k4}}\end{cases}\quad\begin{cases}S_{k1}=1-S_{k3}\\ S_{k2}=1-S_{k4}\end{cases}}. \qquad (42)$$

The equations of voltages (*a*), (*b*), (*c*) of the three-level inverter, with respect to the midpoint «0» of the input voltage source is expressed as [26, 27]:

$$\begin{cases}V_{a0}=(S_{a1}S_{a2}-S_{a3}S_{a4})V_{dc};\\ V_{b0}=(S_{b1}S_{b2}-S_{b3}S_{b4})V_{dc};\\ V_{c0}=(S_{c1}S_{c2}-S_{c3}S_{c4})V_{dc}.\end{cases} \qquad (43)$$

The compound voltages in matrix form are:

$$\begin{bmatrix}V_{ab}\\ V_{bc}\\ V_{ac}\end{bmatrix}=\begin{bmatrix}v_{a0}-v_{b0}\\ v_{b0}-v_{c0}\\ v_{a0}-v_{c0}\end{bmatrix}= \\ =\begin{bmatrix}1&-1&0\\ 0&1&-1\\ -1&0&1\end{bmatrix}\cdot\begin{bmatrix}S_{a1}S_{a2}-S_{a3}S_{a4}\\ S_{b1}S_{b2}-S_{b3}S_{b4}\\ S_{c1}S_{c2}-S_{c3}S_{c4}\end{bmatrix}\cdot V_{dc}. \qquad (44)$$

We can define the simple voltages (v_a, v_b, v_c) with respect to the neutral point *n*:

$$\begin{cases}v_a=v_{an}=v_{a0}-v_{n0};\\ v_b=v_{bn}=v_{b0}-v_{n0};\\ v_c=v_{cn}=v_{c0}-v_{n0}.\end{cases} \qquad (45)$$

The voltage equation between the midpoint of the DC power supply of the inverter and the point load neutral which is written as follows:

$$v_{n0}=\frac{1}{3}(v_{a0}+v_{b0}+v_{c0}). \qquad (46)$$

Finally, the system in the matrix form is:

$$\begin{bmatrix}v_a\\ v_b\\ v_c\end{bmatrix}=\frac{1}{3}\begin{bmatrix}2&-1&-1\\ -1&2&-1\\ -1&-1&2\end{bmatrix}\cdot\begin{bmatrix}S_{a1}S_{a2}-S_{a3}S_{a4}\\ S_{b1}S_{b2}-S_{b3}S_{b4}\\ S_{c1}S_{c2}-S_{c3}S_{c4}\end{bmatrix}V_{dc}, \qquad (47)$$

where S_{k1}, S_{k2}, S_{k3}, S_{k4} are the switching states of the inverter power switches; v_{a0}, v_{b0}, v_{c0} are the phase-to-neutral voltages at the output of the inverter between the phases of the load and the midpoint «0»; v_{n0} is the voltage between the midpoint of the inverter DC supply and the neutral point of the load; v_{an}, v_{bn}, v_{cn} are the phase-to-neutral voltages with respect to the neutral point *n*.

Depending on the states of the inverter, this vector can take several positions in; these positions are designated on the vector diagram or switch hexagon shown in Fig. 7 [24, 26].

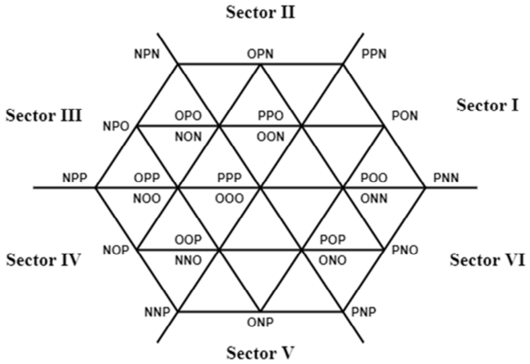

Fig. 7. Space vector diagram of a 3-L NPC inverter

2. Implementation predictive current control. The proposed predictive control strategy is based on the fact that only a finite number of possible switching states can be generated by a power converter static and that models of the system can be used to predict behavior variables for each switching state. For switching selection appropriate to apply, a selection criterion must be defined. This selection criterion is expressed as a quality function that will be evaluated for the predicted values variables to control. The prediction of the future value of these variables is calculated for each possible switching state. The switching state that minimizes the quality function is selected [28, 29]. This approximation is considered in Fig. 8.

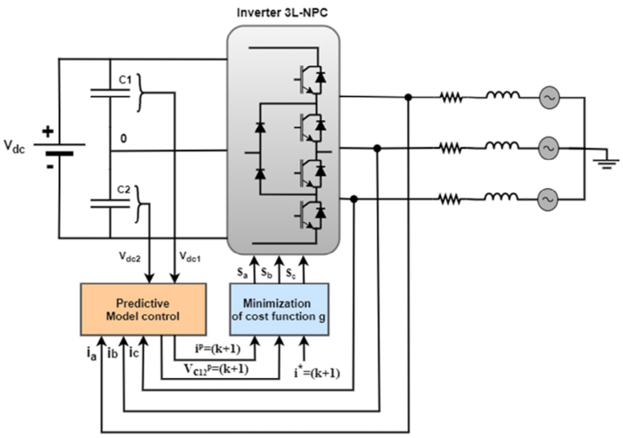

Fig. 8. Block diagram of predictive current control for a 3L-NPC inverter connected to grid

The system model equations are given as follows:

$$\begin{cases} v_{an} = Ri_a + L\dfrac{\mathrm{d}i_a}{\mathrm{d}t} - e_a; \\ v_{bn} = Ri_b + L\dfrac{\mathrm{d}i_b}{\mathrm{d}t} - e_b; \\ v_{cn} = Ri_c + L\dfrac{\mathrm{d}i_c}{\mathrm{d}t} - e_c. \end{cases} \tag{48}$$

After the Clarke transformation and with the use of Euler's method to obtain a discrete-time model of the current, the current equations are expressed as follows:

$$\frac{\mathrm{d}i}{\mathrm{d}t} = \frac{i(k+1) - i(k)}{T_s}, \tag{49}$$

where T_s is the sampling period and k shows sampling time.

$$\begin{cases} i_\alpha^p(k+1) = \left(1 - T_s\dfrac{R}{L}\right) i_\alpha(k) + \dfrac{T_s}{L}\left(v_\alpha - e_\alpha(k)\right); \\ i_\beta^p(k+1) = \left(1 - T_s\dfrac{R}{L}\right) i_\beta(k) + \dfrac{T_s}{L}\left(v_\beta - e_\beta(k)\right). \end{cases} \tag{50}$$

The currents i_{c1}, i_{c2} supplied by each capacitor C_1, C_2 are represented by the following equations:

$$\begin{cases} i_{c1}(k) = i_{dc}(k) - H_{1a}i_a(k) - H_{1b}i_b(k) - H_{1c}i_c(k); \\ i_{c2}(k) = i_{dc}(k) - H_{2a}i_a(k) - H_{2b}i_b(k) - H_{2c}i_c(k). \end{cases} \tag{51}$$

The switch states function of the 3L-NPC calculates the variables (H_{1x}, H_{2x}) and is given by:

$$\begin{cases} H_{1x} = \begin{cases} 1 & \text{if} \quad S_x = \text{"+"}; \\ 0 & \text{other;} \end{cases} \\ H_{2x} = \begin{cases} 1 & \text{if} \quad S_x = \text{"–"}; \\ 0 & \text{other.} \end{cases} \end{cases} \tag{52}$$

We use the Euler method to obtain the equations in discrete time which allows the prediction of DC bus voltages as follows:

$$\begin{cases} v_{c1}^p(k+1) = v_{c1}(k) + \dfrac{1}{C} i_{c1}(k) T_s; \\ v_{c2}^p(k+1) = v_{c2}(k) + \dfrac{1}{C} i_{c2}(k) T_s, \end{cases} \tag{53}$$

where $i(k)$ is i_α^p, i_β^p and represents the current vector in stationary frame α-β; i_{c1}, i_{c2} are the currents flowing respectively through the capacitors C_1, C_2; variables H_{1x}, H_{2x} depend on the switching states; v_{c1}, v_{c2} are the voltages across DC-link capacitors C_1, C_2.

3. Cost function. The objective of the current control scheme is to minimize the error between the currents measured and reference values. This requirement can be written as a cost function. The cost function is expressed in orthogonal coordinates and measures the error between the references and the predicted currents:

$$g = \left|i_\alpha^* - i_\alpha^p\right| + \left|i_\beta^* - i_\beta^p\right| + \lambda_{dc}\left|v_{c1}^p - v_{c2}^p\right|, \tag{54}$$

where g is the cost function; λ_{dc} is the weighting factor.

The evaluation of the precomputed results and the determination of future optimal control actions are made by the cost function [30-33].

4. Diagram smart current control. Predictive model algorithm applied to control the centralized 3L-NPC inverter in WECS is shown in Fig. 9. To make the necessary calculation of the equations of the predictive command Fig. 9 presents the algorithm of the deferent step of this smart control [28, 29].

Results. This section is to validate the results obtained from the model smart predictive current control of 3L-NPC inverter algorithm of WECS through eigenvalues analysis and also the comparative studies between the proposed model and the exist solution already used for PMSG connected to grid. In the first part, the results obtained after rotor side converter are illustrated in Fig. 8.

Figures 10,*a*,*d* show the applied variable change of wind profile for the studied system. Figure 10,*c* presents the form of the DC link voltage. The DC link voltage reference is set to 540 V, the measured voltage perfectly follows the reference signal.

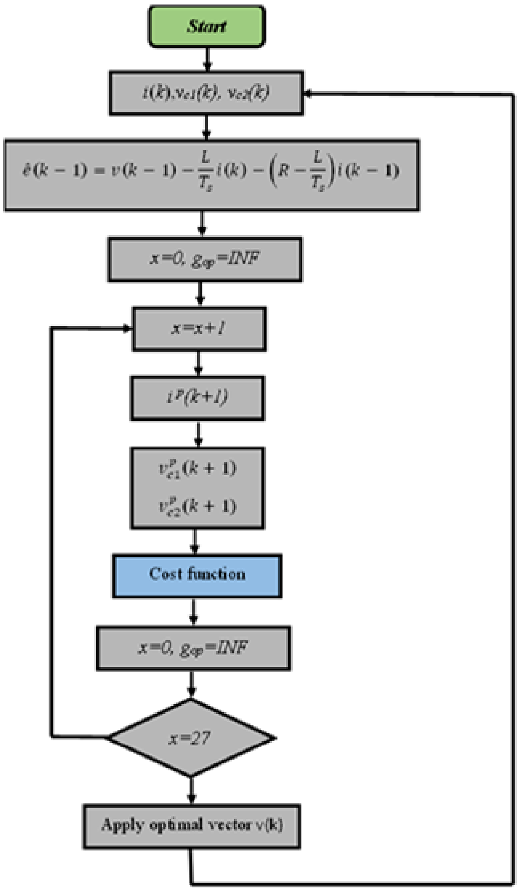

Fig. 9. Smart current control algorithm

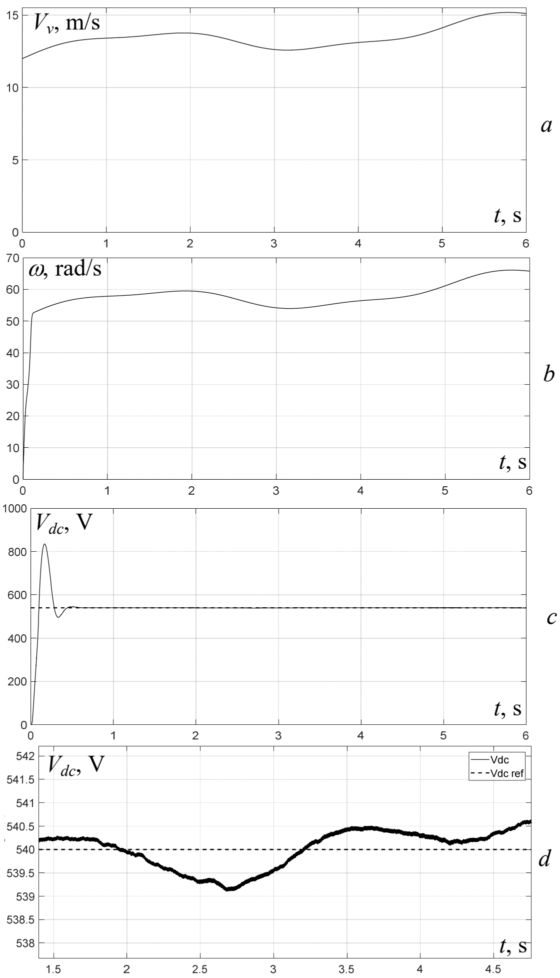

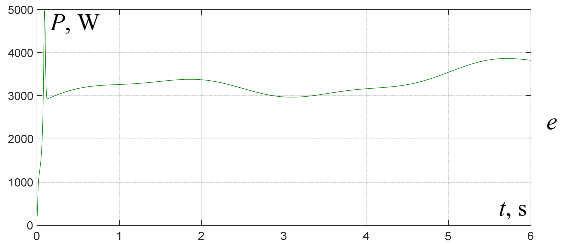

Fig. 10. Simulation results of the rotor side converter:
a – wind speed; *b* – mechanical speed; *c* – DC-link voltage;
d – zoom DC-link voltage; *e* – PMSG power

The second part shows the results after grid side converter and is illustrated in Fig. 11.

Figure 11,*a* clearly shows the proper tracking of the converter reference currents with small currents ripples.

It can be seen in Fig. 9,*b* waveform of the controlled currents i_α and i_β is smooth and stable.

Figure 11,*c* illustrates the DC voltage ripples are low enough. The spectral analysis of the modulated voltage signal is presented in Fig. 11,*g*, where we noticed a drop in Total Harmonic Distortion (THD).

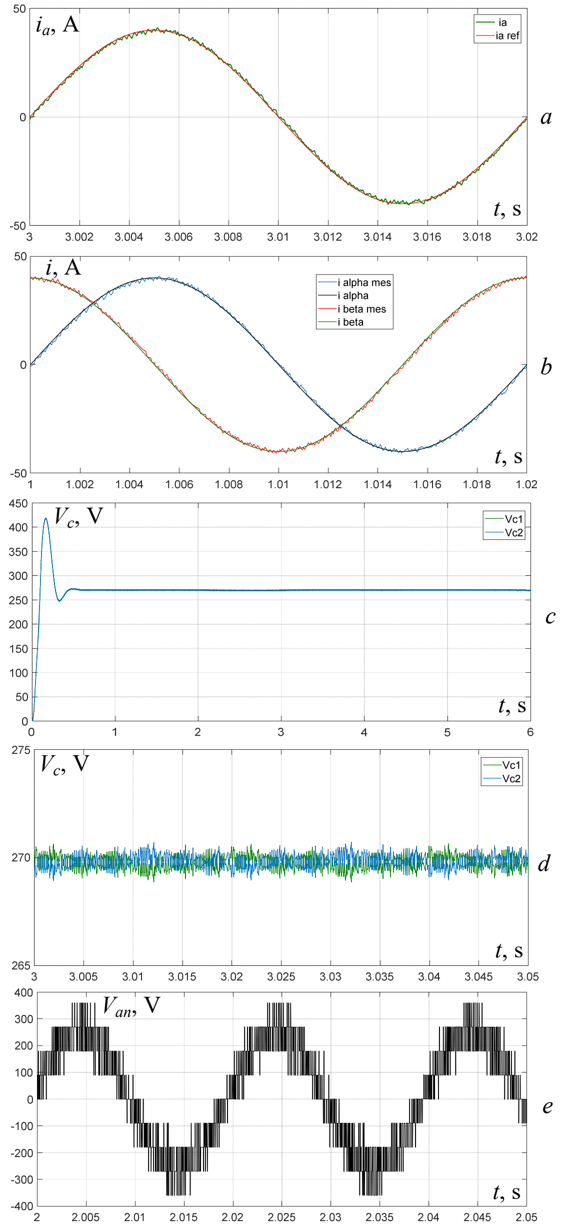

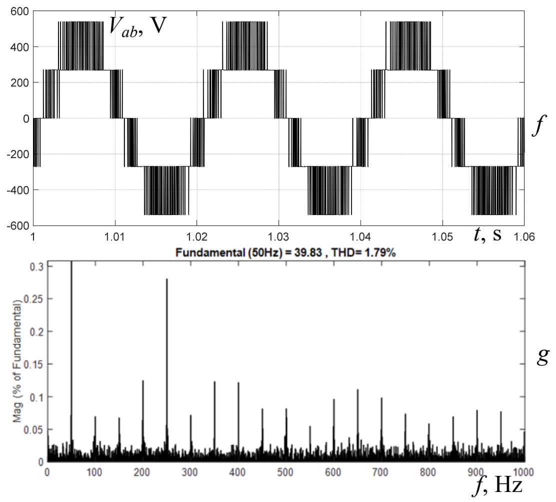

Fig. 11. Simulation results of the grid side converter:
a – output current i_a; *b* – controlled currents i_α, i_β and their references; *c* – DC voltages across the two capacitors V_{dc1}, V_{dc2}; *d* – zoom of the DC voltages across the two capacitors V_{dc1}, V_{dc2}; *e* – simple voltage at inverter output V_{an}; *f* – output line-to-line voltage V_{ab}; *g* – spectrum of current i_a

Comparison to state-of-the-art. The purpose of this part a comparative study between the smart current control of the WECS and exist solution using in [11]. Table 3 summarizes the principal differences between exist solution and the new smart current control of the WECS.

These results and comparison showed high stability, fast response, low disturbance, eases of implementation and strong the robustness of this smart current control.

Table 3
Comparison of smart current control and exist solution

Parameter	Exist solution [11]	Smart current control
Answer dynamic	Stable	Stable
The behavior of current in regime const THD, %	5.3	1.38
Frequency of switching, Hz	2500	2500
Response time, ms	>40	40
Robustness, %	45	80
Complexity of implantation, %	35	10

Conclusions.

1. In this paper, a new design and intelligent control has been proposed and implemented for wind energy conversion system based PMSG.

2. All presented results have validated the capability and effectiveness of the proposed intelligent control strategy and showed a high performance and dynamic behavior even at high power. Also, the measured DC voltage follows the reference voltage closely (transitory response 30 ms) and this proves its robustness. The control of three level neutral point clamped inverter is guaranteed by smart advanced current control, which gives good results regarding THD (1.38 %) in the both of simulation and experimentation results.

3. Optimizing using metaheuristic algorithms are more precise for THD optimization and switching loss mitigation.

4. Experimental validation is the focus of future work: using DC machine for creating mechanical speed of the turbine, multiplier, PMSG, PWM rectifier, board Dspace1104, current sensors, voltage sensors, DC voltage stabilizer, control interface, three level neutral point clamped inverter, MATLAB/Simulink and control desk.

Conflict of interest. The authors of the article declare that there is no conflict of interest.

REFERENCES

1. Sathish C., Chidambaram I.A., Manikandan M. Intelligent cascaded adaptive neuro fuzzy interface system controller fed KY converter for hybrid energy based microgrid applications. *Electrical Engineering & Electromechanics*, 2023, no. 1, pp. 63-70. doi: https://doi.org/10.20998/2074-272X.2023.1.09.

2. Chen R., Ke D., Sun Y., Chung Y.C., Wu H., Liao S., Xu J., Wei C. Hierarchical Frequency-dependent Chance Constrained Unit Commitment for Bulk AC/DC Hybrid Power Systems with Wind Power Generation. *Journal of Modern Power Systems and Clean Energy*, 2023, vol. 11, no. 4, pp. 1053-1064. doi: https://doi.org/10.35833/MPCE.2022.000138.

3. Kamel Eddine Z.H., Dib R., Abed K. New Intelligent Power Adjustment of the Wind Energy Conversion System Extended Virtual Flux based Direct Power Control Using New Fuzzy-PI Controller. *Proceedings of the 9th International Workshop on Simulation for Energy, Sustainable Development & Environment (SESDE 2021)*, 2021, pp. 27-37. doi: https://doi.org/10.46354/i3m.2021.sesde.004.

4. Bhattacherjee H., Mukherjee D., Chakraborty C. Three-level Vienna Rectifier with a Brushless and Permanent Magnetless Generator for Wind Energy Conversion Systems. *Power Electronics and Drives*, 2022, vol. 7, no. 1, pp. 84-102. doi: https://doi.org/10.2478/pead-2022-0007.

5. Choudhury S., Bajaj M., Dash T., Kamel S., Jurado F. Multilevel Inverter: A Survey on Classical and Advanced Topologies, Control Schemes, Applications to Power System and Future Prospects. *Energies*, 2021, vol. 14, no. 18, art. no. 5773. doi: https://doi.org/10.3390/en14185773.

6. Devineni G.K., Ganesh A. Problem Formulations, Solving Strategies, Implementation Methods & Applications of Selective Harmonic Elimination for Multilevel Converters. *Journal Européen Des Systèmes Automatisés*, 2020, vol. 53, no. 6, pp. 939-952. doi: https://doi.org/10.18280/jesa.530620.

7. Eroğlu H., Cuce E., Mert Cuce P., Gul F., Iskenderoğlu A. Harmonic problems in renewable and sustainable energy systems: A comprehensive review. *Sustainable Energy Technologies and Assessments*, 2021, vol. 48, art. no. 101566. doi: https://doi.org/10.1016/j.seta.2021.101566.

8. Sarker R., Datta A., Debnath S. FPGA-Based High-Definition SPWM Generation With Harmonic Mitigation Property for Voltage Source Inverter Applications. *IEEE Transactions on Industrial Informatics*, 2021, vol. 17, no. 2, pp. 1352-1362. doi: https://doi.org/10.1109/TII.2020.2983844.

9. Jayakumar V., Chokkalingam B., Munda J.L. A Comprehensive Review on Space Vector Modulation Techniques for Neutral Point Clamped Multi-Level Inverters. *IEEE Access*, 2021, vol. 9, pp. 112104-112144. doi: https://doi.org/10.1109/ACCESS.2021.3100346.

10. Wu M., Li Y.W., Konstantinou G. A Comprehensive Review of Capacitor Voltage Balancing Strategies for Multilevel Converters Under Selective Harmonic Elimination PWM. *IEEE Transactions on Power Electronics*, 2021, vol. 36, no. 3, pp. 2748-2767. doi: https://doi.org/10.1109/TPEL.2020.3012915.

11. Alakkad M.A.M., Rasin Z., Rasheed M., Abd Halim W., Omar R. Real-time switching thirteen-level modified CHB-Multilevel inverter using artificial neural network technique based on selective harmonic elimination. *Indonesian Journal of Electrical Engineering and Computer Science*, 2020, vol. 20, no. 3, pp. 1642-1652. doi: https://doi.org/10.11591/ijeecs.v20.i3.pp1642-1652.

12. Sami I., Ullah S., Ali Z., Ullah N., Ro J.-S. A Super Twisting Fractional Order Terminal Sliding Mode Control for DFIG-Based Wind Energy Conversion System. *Energies*, 2020, vol. 13, no. 9, art. no. 2158. doi: https://doi.org/10.3390/en13092158.

13. Boukadoum A., Bouguerne A., Bahi T. Direct power control using space vector modulation strategy control for wind energy conversion system using three-phase matrix converter. *Electrical Engineering & Electromechanics*, 2023, no. 3, pp. 40-46. doi: https://doi.org/10.20998/2074-272X.2023.3.06.
14. Bouraghda S., Sebaa K., Bechouat M., Sedraoui M. An improved sliding mode control for reduction of harmonic currents in grid system connected with a wind turbine equipped by a doubly-fed induction generator. *Electrical Engineering & Electromechanics*, 2022, no. 2, pp. 47-55. doi: https://doi.org/10.20998/2074-272X.2022.2.08.
15. Cheikh R., Boualem B., Belmili H. Improved Fuzzy Logic MPPT Controller of Stand-alone WECS-based PMSG under Stochastic Wind Environment. *Journal of Renewable Energies*, 2023, vol. 1, no. 1, pp. 31-42. doi: https://doi.org/10.54966/jreen.v1i1.1096.
16. Ghanem S., Fandi G., Kyncl J., Müller Z. A novel scheme for control by active and reactive power utilized in gearless variable speed wind turbine system with PMSG connected to the grid. *Electrical Engineering & Electromechanics*, 2022, no. 2, pp. 56-68. doi: https://doi.org/10.20998/2074-272X.2022.2.09.
17. Babu A., Shivaleelavathi B.G., Yatnalli V. Efficiency Analysis and Design Considerations of a Hysteretic Current Controlled Parallel Hybrid Envelope Tracking Power Supply. *Engineering, Technology & Applied Science Research*, 2023, vol. 13, no. 1, pp. 9812-9818. doi: https://doi.org/10.48084/etasr.5414.
18. Sakri D., Laib H., Farhi S.E., Golea N. Sliding mode approach for control and observation of a three phase AC-DC pulse-width modulation rectifier. *Electrical Engineering & Electromechanics*, 2023, no. 2, pp. 49-56. doi: https://doi.org/10.20998/2074-272X.2023.2.08.
19. Malinowski M. *Sensorless Control Strategies for Three-Phase PWM Rectifiers*. Ph.D. Thesis, Faculty of Electrical Engineering Institute of Control and Industrial Electronics, Warsaw University of Technology, 2001. 128 p.
20. Deng Q., Gou B., Ge X., Lin C., Xie D., Feng X. A High-Accuracy-Light-AI Data-Driven Diagnosis Method for Open-Circuit Faults in Single-Phase PWM Rectifiers. *IEEE Transactions on Transportation Electrification*, 2023, vol. 9, no. 3, pp. 4352-4365. doi: https://doi.org/10.1109/TTE.2023.3238009.
21. Zhou Z., Song J., Yu Y., Xu Q., Zhou X. Research on High-Quality Control Technology for Three-Phase PWM Rectifier. *Electronics*, 2023, vol. 12, no. 11, art. no. 2417. doi: https://doi.org/10.3390/electronics12112417.
22. Kendouli F., Nabti K., Labed K., Benalla H. Modélisation, simulation et contrôle d'une turbine éolienne à vitesse variable basée sur la génératrice asynchrone à double alimentation. *Journal of Renewable Energies*, 2023, vol. 14, no. 1, pp. 109-120. (Fra). doi: https://doi.org/10.54966/jreen.v14i1.245.
23. Adjie A.P., Hamid M.I. Harmonics Analysis of Input Current of 3-Phase PWM Rectifier. *Andalas Journal of Electrical and Electronic Engineering Technology*, 2021, vol. 1, no. 1, pp. 31-40. doi: https://doi.org/10.25077/ajeeet.v1i1.6.
24. Yaramasu V. *Predictive control of multilevel converters for megawatt wind energy conversion systems*. PhD Thesis, Ryerson University, Toronto, ON, Canada, 2014. 259 p. doi: https://doi.org/10.32920/ryerson.14655330.v1.
25. Abid M., Laribi S., Larbi M., Allaoui T. Diagnosis and localization of fault for a neutral point clamped inverter in wind energy conversion system using artificial neural network technique. *Electrical Engineering & Electromechanics*, 2022, no. 5, pp. 55-59. doi: https://doi.org/10.20998/2074-272X.2022.5.09.
26. Guo F., Ma Z., Diao F., Zhao Y., Wheeler P. Hybrid Virtual Coordinate-Driven CBPWM Strategy of Three-Level T-Type NPC Converters for Electric Aircraft Propulsion Applications. *IEEE Transactions on Industrial Electronics*, 2024, vol. 71, no. 3, pp. 2309-2319. doi: https://doi.org/10.1109/TIE.2023.3266552.
27. Lyu J., Yan H., Ding J., Wu Q., Lyu X., Sun Z. Optimal switching sequence model predictive control for three-level NPC grid-connected inverters. *IET Power Electronics*, 2021, vol. 14, no. 3, pp. 626-639. doi: https://doi.org/10.1049/pel2.12050.
28. Gu X., Xu W., Zhang G., Chen W., Jin X. Three-Level Inverter-PMSM Model Predictive Current Control Based on the Extended Control Set. *Electronics*, 2023, vol. 12, no. 3, art. no. 557. doi: https://doi.org/10.3390/electronics12030557.
29. Vargas R., Cortes P., Ammann U., Rodriguez J., Pontt J. Predictive Control of a Three-Phase Neutral-Point-Clamped Inverter. *IEEE Transactions on Industrial Electronics*, 2007, vol. 54, no. 5, pp. 2697-2705. doi: https://doi.org/10.1109/TIE.2007.899854.
30. Rodriguez J., Pontt J., Silva C.A., Correa P., Lezana P., Cortes P., Ammann U. Predictive Current Control of a Voltage Source Inverter. *IEEE Transactions on Industrial Electronics*, 2007, vol. 54, no. 1, pp. 495-503. doi: https://doi.org/10.1109/TIE.2006.888802.
31. Rojas D., Rivera M., Munoz J., Baier C., Wheeler P. Predictive Current Control Applied to a 3L-NPC Inverter. *2021 IEEE International Conference on Automation/XXIV Congress of the Chilean Association of Automatic Control (ICA-ACCA)*, 2021, pp. 1-7. doi: https://doi.org/10.1109/ICAACCA51523.2021.9465309.
32. Babes B., Hamouda N., Kahla S., Amar H., Ghoneim S.S.M. Fuzzy model based multivariable predictive control design for rapid and efficient speed-sensorless maximum power extraction of renewable wind generators. *Electrical Engineering & Electromechanics*, 2022, no. 3, pp. 51-62. doi: https://doi.org/10.20998/2074-272X.2022.3.08.
33. Katkout A., Nasser T., Essadki A. An Efficient Model Predictive Current Control Algorithm for Grid-Connected Multi-Level Inverter with Computational Delay Compensation. *2020 International Conference on Electrical and Information Technologies (ICEIT)*, 2020, pp. 1-6. doi: https://doi.org/10.1109/ICEIT48248.2020.9113234.

Received 25.07.2023
Accepted 10.11.2023
Published 02.03.2024

Hamed Kamel Eddine Zine[1], *PhD Student,*
Khoudir Abed[1], *PhD, Master of Computer Application,*
[1] Department of Electrical Engineering,
Faculty of Engineering Sciences,
Laboratory of Electrical Engineering of Constantine (LGEC),
Mentouri University, Road Ain El Bey, Constantine, Algeria,
e-mail: kamel-eddine.zine-hamed@lec-umc.org,
khoudir.abed@laposte.net (Corresponding Author)

How to cite this article:
Zine H.K.E., Abed K. Smart current control of the wind energy conversion system based permanent magnet synchronous generator using predictive and hysteresis model. *Electrical Engineering & Electromechanics*, 2024, no. 2, pp. 40-47. doi: https://doi.org/10.20998/2074-272X.2024.2.06